Dear Editor,

On behalf of all co-authors, I am sending you the revised version of our manuscript taking into account the constructive criticism of the six referees. Based on the comments from the six reviewers, we restructured the manuscript and revised the figures accordingly. We hope we responded satisfactorily to all reviewers' comments and requests, and that these changes have greatly improved the manuscript. Please find the revised version of our manuscript cp-2018-159 with changes highlighted using colored text in answer to specific comments.

We are looking forward hearing from you and if you have any further queries please do not hesitate to contact me.

Yours sincerely,

Bassem Jalali

Influence of the North Atlantic subpolar gyre circulation on the 4.2 ka BP event

Bassem Jalali[1], Marie-Alexandrine Sicre[1], Julien Azuara[2], Violaine Pellichero[1] and Nathalie Combourieu-Nebout[2]

[1]LOCEAN Laboratory, Sorbonne Universités (UPMC, Univ Paris 06)-CNRS-IRD-MNHN, Paris, France.

[2]Histoire naturelle de l'Homme Préhistorique (UMR 7194 CNRS), Département Homme et Environnement, Muséum national d'Histoire naturelle, Institut de Paléontologie humaine, France.

Abstract

The 4.2 ka BP event, spanning from ca 4200 to 3900 cal yr BP, has been documented in numerous archaeological data and continental archives across the northern hemisphere as an abrupt shift to dry and cold climate. However, data on synchronous ocean circulation changes are notably lacking thus preventing from getting a full insight into the physical mechanisms responsible for this climate deterioration. Here, we present two high-resolution (5-20 years) sea surface temperature (SST) records from the subpolar gyre and off North Iceland in the vicinity of the polar front obtained from alkenone paleothermometry and compare them with proxy data from the Western Mediterranean Sea to gain information on regional temperature and precipitation patterns. Our results evidence a temperature dipole pattern which, combined with other paleoceanographic records of the North Atlantic, suggests a weakening of the subpolar gyre possibly associated with atmospheric blocked regimes.

I. Introduction

Holocene rapid climate changes (RCCs) are century-long time intervals of enhanced high-latitude cooling and tropical dryness (Mayewski et al., 2004; Wanner et al., 2011). The forcing mechanisms that trigger these RCCs are multiple and in many cases unclear (Wanner et al., 2014). Bond et al. (2001) suggested a relationship between RCCs and the reduction of the North Atlantic deep-water production (NADW) to explain their transmission around the Northern hemisphere. By examining 50 globally distributed proxy records, Mayewski et al. (2004) concluded that RCCs result from natural external forcing (i.e. solar and volcanism) and interactions with internal variability (ocean-atmosphere dynamic). Wanner et al. (2011) highlighted the absence of a clear periodicity of the RCCs and the lack of spatio-temporal homogeneity of temperature and humidity patterns of these events. They also recognized that the early Holocene RCC known as the 8.2 event likely differed from other Holocene RCCs because of anomalously high freshwater forcing and insolation at the final stage of the deglaciation.

The 4.2 ka BP event, developing from 4200 to 3900 yr BP (Weiss, 2016), is one of the most widely documented RCCs. Considered as the second outstanding RCC after the 8.2 ka BP event in terms of magnitude and duration, it is often regarded as a boundary between the Middle and Late Holocene climate (Magny et al, 2013; Walker et al., 2012). It is notably known for being synchronous with the occurrence of a megadrought in the Levant and the collapse of the Akkadian Empire and the Old Kingdom in Egypt, and further East of the Old Chinese cultures (Weiss and Bradley, 2001; Liu and Feng, 2012; Stanley et al., 2003). In the last decade, an increasing number of high-resolution proxy records has provided a more comprehensive description of this event (Weiss, 2016). In the Mediterranean region, climate reconstructions have highlighted a drastic reduction of precipitation and extreme climate conditions prevailing during this period, mostly during the winter season (Magny et al., 2013; Fohlmeister et al., 2013; Zanchetta et al., 2016; Cheng et al., 2015; Ruan et al., 2016; Jalali et al., 2016; Finné et al., 2017; Bini et al., 2019, this issue and references therein). According to Weiss (2015), a 30-50 % reduction of precipitation delivered by the Mediterranean westerlies during the 4.2 ka BP event led to extreme dryness in the Middle East and Central Asia. The synthesis of Weiss (2016) also pointed out a weakening of major monsoon systems during this period. Evidence for Indian monsoon disruption comes from high-resolution speleothem and Lake Rara precipitation records (Berkelhammer et al., 2012; Dixit et al., 2014; Nakamura et al., 2016). Donges et al. (2015) also reported a weakening of East and South-West Asian summer monsoon resulting in pronounced dryness in northeastern China, Inner Mongolia and Australia. Finally, a drastic decline of precipitation was also observed over North America (Booth et al., 2005; Fisher, 2008).

While the expression of the 4.2 ka BP event is evident in several paleoclimatic records all over the northern hemisphere, physical drivers of this climatic period are still not elucidated in part because of missing data from the ocean, the main water and heat reservoir on Earth. Booth et al. (2005) proposed a La Niña -like pattern and warming of the equatorial Atlantic Ocean to explain enhanced dry conditions in North America between 4100 and 4300 yrs BP. Liu et al. (2014) suggested a transition from negative to positive Pacific North American (PNA)-like pattern as an alternative explanation. Transient simulations obtained from the Community Climate System Model (CCSM) of NCAR showed that while modeled large-scale spatial pattern of the 4.2 and 8.2 events reproduce a pronounced cooling and precipitation reduction over the northern hemisphere, operating mechanisms are different (Ning et al. 2019, this issue). According to this study, in the North Atlantic domain, orbital forcing would have caused a weakening of the Atlantic meridional overturning circulation (AMOC) and subsequent cold and dry conditions of the 4.2 event, while freshwater release in the Labrador Sea and subsequent AMOC collapse triggered the 8.2 event. Apart from taking place under different insolation conditions, these two RCCs experienced notably different solar and volcanic forcing. Indeed, the absence of large volcanic eruptions (under strong solar activity) during the 4.2 event contrasts with the intense volcanism of the 8.2 event (Kobashi et al., 2017).

In this paper, we present two unprecedented high-resolution (5-20 years) sea surface temperature (SST) records obtained from alkenone analyses in two sediment cores recovered off North Iceland in the Western Nordic Seas (MD99-2275) and in the subpolar gyre (SPG), South of Iceland (MD95-2015). This study extends the SSTs of the MD99-2275 in part published by Sicre et al. (2008). New pollen data and already published alkenone-SSTs (Jalali et al., 2016) from the KSGC-31 core located in the Gulf of Lion (NW Mediterranean) are also used in the discussion. These records are compared with other regional proxy data from the Euro-Mediterranean region to explore the link between the North Atlantic Ocean circulation and the Western Europe climate during this time span where a disruption of early Mediterranean civilizations was observed.

II. Material and methods

The MD99-2275 core was retrieved off North Iceland in the Western Nordic Seas (66.55°N; 17.7°W, 470 m water depth) in the vicinity of the present day polar front (Fig. 1, site 2) where the warm and salty North Icelandic Irminger Current (NIIC) meets with the cold and fresher waters of the East Icelandic Current (EIC) (Fig. 1). The age model of the MD99-2275 core is based on 15 tephra layers and calculated using the Bayesian approach of OxCal4.2 software (for details see Figure 2 and Table DR4 in Jiang et al., 2015). The second core site MD95-2015 (58.76°N; 25.95°W; 2630 m water depth) is located South of Iceland on the eastern flank of the Reikyanes Ridge (Fig. 1, site 1). The age model is based on 21 ^{14}C dates measured in the planktonic foraminifera *Globigerina bulloides* (Table S1, Figure S1; Kissel et al., 2013). Both cores were collected as part of the international IMAGES program (International Marine Past Global Change Study, http://www.images-pages.org/). The third core KSGC-31 (43°N, 3.29°E; 60 m water depth) was recovered from the Gulf of Lion inner-shelf mud belt during the GM02 Carnac cruise in 2002 (Bassetti et al., 2016). The age model of this core is based on 17 ^{14}C dates measured on bivalve shells (Table S1, Figure S2). For MD95-2015 and KSGC-31 cores, the age model was calculated using the Bayesian Oxcal4.3 software (Ramsey, 2017) and the MARINE13 calibration data set (Reimer et al., 2013). Reservoir ages were obtained from the Global Marine Reservoir Database by averaging the eight nearest site reservoir ages of each core (http://calib.org/marine/), leading to a ΔR = 73±69 yrs for MD95-2015 and 23±71 yrs for KSGC-31.

Both MD95-2015 and MD99-2275 sediment cores (Fig. 1, sites 1 and 2 respectively) were continuously sampled at a sampling step of 1 cm for alkenone biomarker analysis. Lipids were extracted from a few grams of freeze-dried sediments following the experimental procedure adapted from Ternois et al. (1997). Alkenones were isolated from the total lipid extract by silica gel chromatography and quantified using a Varian CX 3400 gas chromatograph after the addition of a known amount of 5α-cholestane used as an external standard. SSTs were derived from the unsaturation index of C_{37} alkenones $U^{K'}_{37} = (C_{37:2})/(C_{37:2} + C_{37:3})$ and the calibration of Prahl et al. (1988), $T = (U^{K'}_{37} - 0.039)/0.034$. $C_{37:4}$ was absent in core MD95-2015 and present in minor amounts in some horizons in the MD99-2275. Based on the age models of the two cores, the mean temporal resolution is estimated to 5 years for MD99-2275 and 20 years for MD95-2015. Internal precision for SST estimates is on the order of 0.5°C.

Pollen for the KSGC-31 core (Fig. 1, site 10) were generated from 25 samples taken in the 4.2 ka time interval to obtain complementary information on vegetation changes in relation with precipitation that took place in the catchment area of the Gulf of Lion. The pollen extraction procedure follows the standard method modified from Faegri and Iversen (1989) (for details see Combourieu-Nebout et al., 1999). Pollen counting was performed on around 300 grains (more than 100 if we except Pinus grains) at x500 magnification while pollen grains were identified at x1000 magnification and compared to pollen atlases (Beug, 2004, Reille, 1992). Pollen percentages were calculated after ruling out Pinus pollen because of their over-representation in marine sediments (Combourieu-Nebout et al., 1999, 2013 and reference therein). Pollen in this core site originates from a large catchment area thus providing an integrated picture of the vegetation from the coastline to the top of the nearby mountains. In this study, we use the log of the *Fagus/*deciduous *Quercus* ratio to assess precipitation changes. Indeed, it has been shown by Quezel, (1979) that *Fagus* develops mainly in the French Mediterranean mountains, thought at the limit of its geographical range in terms of precipitation requirements (>750 mm). Because deciduous *Quercus* is more tolerant to dryness than *Fagus*, decreasing *Fagus/*deciduous *Quercus* ratio values presumably reflect increasing aridity (Azuara et al., 2015). The Holocene SST record of the core has been published by Jalali et al. (2016). Based on the age model of KSGC-31 core, the mean temporal resolution is 15 years for SST record and 44 years for pollen data.

III. Results and discussion

As shown in Figure 2, the sea surface temperature (SST) signal of the MD99-2275 core contains strong decadal scale variability with values ranging between 7 and 10°C around a mean value of 9°C. Within the 4.2 ka BP event interval, shaded in grey, SSTs show an overall cooling of ~2°C and a small amplitude temperature reversal around 4200 yr BP followed by an abrupt decline to coldest values (6.7°C) at ~ 4100 yr BP. South of Iceland, SSTs fluctuate between 9 and 12°C, thus in a warmer range than off North Iceland as expected from the core locations. They also show marked multi-centennial oscillations of 1 to 2°C amplitude but of broadly opposite sign than off North Iceland, with a maximum value of 12°C reached around 4100 yr BP. The C_{37} alkenone concentrations used to derive SSTs in MD95-2015 are on average 334 ng/g (range 36 to 700 ng/g) (Fig. 2c). Those found in MD99-2275 range from 20 to 1000 ng/g, with a mean value of 362 ng/g (Fig. 2d). In both case alkenone abundances were high enough to calculate reliable SSTs.

III.1. Evidence of weak North Atlantic SPG circulation during the 4.2 ka BP event

Figure 3 compares our SST data (fig. 3a, b) and other records from North Atlantic sediments (Fig. 1) which include the proxy reconstruction of the SPG intensity of Thornalley et al. (2009) (Fig. 3c) and the mean grain size of sortable silt (SS; 10-63µm) from Gardar drift sediments of Mjell et al. (2015) used as a proxy of the strength of the Iceland-Scotland Overflow Water (ISOW) (Fig. 3d). Also shown are the Na fluxes from GISP2 ice core (Fig. 3e) (O'Brien et al., 1995) reflecting changes in atmospheric circulation. Additional information on surface ocean circulation changes is provided by the reconstructions of sea-ice concentration over the East Greenland shelf (Fig 3f) and of the surface salinity in the Labrador Sea (Fig. 3g) (Solignac et al., 2004; 2006). Finally, summer SSTs derived from diatom assemblages (Fig. 3h) were used to assess variations of the warm Atlantic inflow into the Nordic Seas (Berner et al., 2011). These surface water property and proxy reconstructions of dynamical parameters were combined to investigate North Atlantic circulation changes during the 4.2 ka BP event.

As emphasized in the previous section, warm SSTs in the subpolar gyre region contrast with the cold surface waters in the Nordic Seas during the 4.2 ka BP event (Figs. 3a and b). The same temperature pattern was also evidenced during the Little Ice Age (LIA), the most recent of the Holocene RCCs. Based on model simulations and proxy data Moreno-Chamarro et al. (2017) demonstrated that this temperature dipole fingerprints a weakening of the SPG, which in turn created the conditions for atmospheric blocking over the Northeastern Atlantic (Häkkinen et al., 2011) responsible for severe winters in Europe during the LIA (Luterbacher et al., 2004). Persistent blocking activity has been shown to also trigger rapid ocean changes such as the Great Salinity Anomaly (GSA) in the 1970s. Indeed, blocking over Greenland by enhancing sea ice export from the Arctic Ocean through Fram Strait produces a freshening of the Labrador Sea several years later, the decline of convection and slowdown of the SPG (Ionita et al., 2016). However, the role of external forcing (solar and volcanism) during the LIA remains an open question (Moffa-Sanchez et al., 2014; Moreno-Chamarro et al., 2016; 2017). Available transient simulations of the 4.2 ka BP event performed with the Community Climate System model version 3 (CCSM3) suggest that internal variability (North Atlantic Oscillation; NAO) could have been played an essential role in the SPG circulation change, with possible modulation by external forcings (Yan and Liu, 2019, this issue; Ning et al., 2019, this issue) but none of these simulations have used solar and volcanic forcings. In the following, we explore the hypothesis of a reduction of the SPG and causal links between sea ice, wind intensity and AMOC to explain our results.

Figure 3c shows the reconstruction of the SPG strength based on the water density difference between surface and subsurface waters obtained from paired Mg/Ca and $\delta^{18}O$ measurements performed on *Globigerina bulloides* and *Globorotalia inflata*, respectively (Thornalley et al., 2009). This density difference reflects the degree of stratification of the upper ocean due to the respective contribution of the North Atlantic Inflow and Polar waters. Lower (higher) and decreasing (increasing) values of the water density difference between surface and subsurface layers are indicative of a slowdown (strengthening) of the SPG. This index indicates a gradual decrease of the SPG from 5400 yr BP to 4200-4100 yr BP. The parallel decline of the ISOW intensity inferred from the mean SS suggests a slowdown of AMOC (Fig. 3d) (Mjell et al 2015) that is supported by cooling of summer SSTs off Norway (Fig. 1, site 9 and 3h; Berner et al., 2011). All together, these reconstructions indicate a progressive slowdown of the SPG and AMOC between 5400 and 4200-4100 yr BP and consecutive northward ocean heat transport reduction leading to cold conditions in the Nordic seas.

Freshwater export from the Arctic Ocean and wind stress are important controlling factors of the SPG circulation through deep convection in the Labrador Sea (Langehaug et al., 2012; Born and Stocker, 2014). Increase sea salt Na flux in Greenland ice core has been related to the expansion of the polar vortex and/or enhance meridional wind flow. The co-eval weakening of the SPG and negative trend of the Na fluxes till approximately 4200-4300 yr BP can be explained either by a decrease in wind intensity or more sea ice both acting to reduce the production of sea salt aerosols (Fig. 3e). Available proxy records of sea ice out of the Arctic Ocean through Fram Strait for this period are scarce. However, the low-resolution time series from South of the Denmark Strait based on dinoflagellate cyst assemblages suggest that the 4500-3900 yr BP interval would have been a long-standing period with almost no sea ice (Fig. 3f; Site 6 in Fig. 1; Solignac et al., 2006). The diminished influence of Polar Waters is also supported by increasing sea surface salinity in the Labrador Sea between 4800 and 4000 yr BP (Fig. 3g; site 5 in Fig. 1; Solignac et al., 2004). Both proxy reconstructions therefore point to a weak East Greenland Current (EGC) along the East Greenland coast during this time period (Solignac et al., 2006; De Vernal et al., 2013).

Paleodata as well as modern observations have also shown that in a weak state, the SPG is confined to the western part of the basin and has a North/South orientation favoring the

Irminger Current (IC) inflow to the SE Greenland/NW Iceland shelf (Hátún et al., 2005; Andresen et al., 2012). Such incursions of warm IC water have notably been evidenced by high occurrences of the benthic foraminifera *Cassidulina neoteretis* between 5200 and 4200 yr BP at the core Fox05R/04G site by Andresen et al. (2012) (site 8 in Fig. 1). A weak SPG induces a surface cooling in the Nordic seas due to decreased heat transport thereby promoting the expansion of sea ice cover especially in the Nordic and Barents seas (Moreno-Chamarro et al., 2017). This is in agreement with the long-term cooling of Nordic Seas reported by Berner et al. (2011) along the Norwegian coast (Fig. 3h) and the increase abundance of sea-ice diatoms between 4300 and 4100 yr BP in MD99-2275 that parallels the alkenone SSTs decrease (Ran et al., 2008). Note that these authors further specified that this increase was marginally due to Arctic sea-ice diatoms, which further supports the assumption of a low Arctic water influence. Instead, local sea ice formation would have been favored by colder conditions. Sea ice concentration in the Barents Sea show consistent increasing values since 4600 yr BP (De Vernal et al., 2013) as opposed to SE Greenland and Labrador Sea, in agreement with the SST dipole featuring a weak SPG. The 4.2 ka BP event would thus differ from the LIA marked by the return of sea ice and the southeastern expansion of the Polar Front (Massé et al., 2008; Sha et al., 2016). Although proxy records of the 4.2 ka BP event suggest a reduction of the SPG, ISOW and possibly of the AMOC, the mechanisms involved are likely to be different because of less severe sea ice conditions and feedbacks as well as external forcing. In the next section we discuss the climatic expression of the 4.2 ka BP event in the Euro-Mediterranean region based on continental record of concomitant hydroclimate changes.

III.2. Climatic expression in the Euro-Mediterranean region

Figure 4 shows high-resolution SST and pollen records from the Gulf of Lion together with the oxygen isotope signals of two stalagmites from the western Mediterranean sensitive to continental precipitation (Zanchetta et al., 2016; Ruan et al., 2016). SSTs in the Gulf of Lion (site 10 in Fig. 1) reveal a ~2°C cooling between 4400 and 3800 yr BP, with two brief colder intervals around 4300 and 4100 yr BP that seem to coincide with the colder SSTs seen off North Iceland. Yet cooling at 4100 yr BP is sharp and more prominent in the Western Nordic Seas, possibly due to the presence of sea ice (Fig. 4a, d). Coldest SST values in the Gulf of Lion during the LIA have been related to persistent wintertime atmospheric blocking over the NE Atlantic resulting in more intense and colder Mistral winds blowing all year round but more strongly during the winter season (Sicre et al., 2016) that are consistent with the previously discussed North Atlantic paleodata and model simulation results (Moffa-Sanchez et al., 2014; Moreno-Chamarro et al., 2016; 2017). Pollen data were investigated to assess environmental conditions over adjacent continental regions to complement the information provided by SSTs. The *Fagus/Quercus* ratio values between 4400 and 3800 yr BP indicate vegetation changes that reflect broadly wetter conditions with higher representation of *Fagus* (associated with Abies) in the forest. This is in agreement with the same ratio record from the nearby Holocene Palavas Lagoon sediments (site 11 in Fig. 1; Azuara et al, 2015) (Fig 4b,c). A short event centered at 4200 yr BP (and possibly around 3900 yr BP) showing a decrease of *Fagus* in favor of *Quercus* may be indicative of a brief spell of moderate dryness. This change can be related to a lower temperate forest development seen in the central Italy records of Lago di Vico and Lagaccione (Magri and Sadori, 1999; Magri, 1999) and in the Gulf of Gaeta (Di Rita et al., 2018). In central Italy and in the Gulf of Lion, pollen data do not show a significant change in vegetation but only a modification of the forest composition that corresponds to a slight decrease in precipitation (Di Rita and Magri, 2019; this issue). The speleothem data from Italy and Algeria give a more detailed and complex picture of precipitation during the 4.2 ka BP event. The oxygen isotope record from the Renella Cave stalagmite in Italy (Fig. 4e; Zanchetta et al., 2016; site 12 in Fig. 1) and Gueldaman Cave in northern Algeria (Fig. 4f; Ruan et al., 2016; site 13 in Fig. 1) both indicate increasingly drier conditions starting around 4800 yr BP. At Gueldaman Cave, archaeological data indicate the settlement abandonment of the cave by human groups around 4400 yr BP (Ruan et al., 2016). Both site witness marked aridity conditions between 4400 and 3800 yr BP but a distinct slightly wetter period between 4200 and 4100 yr BP. The pollen data in the Gulf of Lion seem to picture a similar complex structure of this interval that however appears to be reflect generally more humid conditions of the catchment basin of the KSGC-31 site. Interestingly, the same double-peak centennial scale cooling and drought have been detected in transient simulations over the past 21,000 years and the dry phases attributed to the presence of anticyclones over Western Europe (Yan and Liu, 2019; this issue). These model results also indicate a southern shit of the ITCZ that is consistent with a weakening of the AMOC.

IV. Conclusions

Unprecedented high-resolution alkenone-derived SST records of the 4.2 ka BP event have been generated from the Western Nordic Seas and North Atlantic sediments in order to explore causes for this cold/dry event of the mid-Holocene and the role of the ocean in the observed changes. The spatial distribution of the SST indicates a cold/warm dipole between 4400 and 3800 yr BP that characterizes a weak SPG, which is supported by other marine proxy records across the North Atlantic. Enhanced wintertime North Atlantic anticyclone blocking induced by a weak subpolar gyre circulation would account for cold and drought conditions. Continental proxy records in Italy and Algeria indicate a double-peak centennial scale structure of the 4.2 ka BP event with prevailing dry conditions interrupted by a slightly wetter period that is also seen in transient model simulations. These numerical experiments suggest a more important role of internal variability and insolation than during the LIA. More investigations are needed to confirm our findings to get a mechanistic understanding of climate during this period.

Acknowledgments

This work was financially supported by the MISTRALS/PaleoMex program. The research leading to this study has received funding from the French National Research Agency HAMOC project (ANR-13-BS06- 0003). We thank Sandrine Canals for the pollen samples processing at ISEM laboratory in Montpellier.

References

Andresen, C. S., Hansen, M. J., Seidenkrantz, M. S., Jennings, A. E., Knudsen, M. F., Nørgaard-Pedersen, N., Larsen, N. K., Kuijpers A., and Pearce, C.: Mid-to late-Holocene oceanographic variability on the Southeast Greenland shelf, The Holocene, 23, 167-178, 2012.

Azuara, J., Combourieu-Nebout, N., Lebreton, V., Mazier, F., Müller, S. D., and Dezileau, L.: Late Holocene vegetation changes in relation with climate fluctuations and human activity in Languedoc (southern France), Clim. Past, 11, 1769-1784, https://doi.org/10.5194/cp-11-1769-2015, 2015.

Bassetti, M-A, Berné, S., Sicre, M.-A., Dennielou B., Alonso Y., Buscail R., Jalali, B., Hebert B., and Menniti, C.: Holocene hydrological changes in the Rhône River (NW Mediterranean) as recorded in the marine mud belt, Clim. Past, 12, 1539–1553, 2016.

Berkelhammer M., Sinha A., Stott L., Cheng H., Pausata F.S.R., and Yoshimura K.: An abrupt shift in the Indian monsoon 4000 years ago, in Giosan L.et al., eds., Climates, landscapes, and civilizations: American Geophysical Union Geophysical Monograph 198, p.75–87, doi:10.1029/2012GM001207, 2012.

Berner, K. S., Koç, N., Godtliebsen, F., and Divine, D.: Holocene climate variability of the Norwegian Atlantic Current during high and low solar insolation forcing, Paleoceanography, 26, PA2220, doi:10.1029/2010PA002002, 2011.

Beug, H. J.: Leitfaden der Pollenbestimmung für Mitteleuropa und angrenzende Gebiete, Verlag Dr. Friedrich Pfeif, München, 542 pp., 2004.

Bini, M. Zanchetta, G., Persoiu, A., Cartier, R., Català, A., Cacho, I., Dean, J. R., Di Rita, F., Drysdale R. N., Finnè, M., Isola, I., Jalali, B., Lirer, F., Magri, D., Masi, A., Marks, L., Mercuri, A.-M., Peyron, O., Sadori, L., Sicre, M.-A., Welc, F., Zielhofer, C., and Brisset, E.: The 4.2 ka BP Event in the Mediterranean Region: an overview, Clim. Past Discuss., https://doi.org/10.5194/cp-2018-147, 2018

Bond, G., Kromer, B., Beer, J., Muscheler, R., Evans, M. N., Showers, W., and Bonani, G.: Persistent solar influence on North Atlantic climate during the Holocene, Science, 294, 2130-2136, 2001.

Booth, R. K., Jackson, S. T., Forman, S. L., Kutzbach, J. E., Bettis III, E. A., Kreig, J., and Wright, D. K.: A severe centennial-scale drought in mid-continental North America 4200 years ago and apparent global linkage, The Holocene, 15, 321-328, 2005.

Born, A., and Stocker, T. F.: Two stable equilibria of the Atlantic subpolar gyre, J. Phys. Oceanogr., 44, 246-264, 2014.

Cheng, H., Sinha, A., Verheyden, S., Nader, F. H., Li, X. L., Zhang, P. Z., ... and Ning, Y. F.: The climate variability in northern Levant over the past 20,000 years, Geophys. Res. Lett., 42,, 8641-8650, 2015.

Combourieu-Nebout, N, Londeix, L, Baudin, F.: Quaternary marine and continental paleoenvironments in the western Mediterranean (Site 976, Alboran Sea): Palynological evidence: In Zahn, R, Comas, MC, Klaus, A. (eds), Proceedings of ODP Scientific Results, 161, College Station, TX: Ocean Drilling Program, 457–468, 1999.

Combourieu-Nebout, N., Peyron, O., Bout-Roumazeilles, V., Goring, S., Dormoy, I., Joannin, S., Sadori, L., Siani, G., and Magny, M.: Holocene vegetation and climate changes in the central Mediterranean inferred from a high-resolution marine pollen record (Adriatic Sea), Clim. Past, 9, 2023-2042, 2013.

De Vernal, A., Hillaire-Marcel, C., Rochon, A., Fréchette, B., Henry, M., Solignac, S., and Bonnet, S.: Dinocyst-based reconstructions of sea ice cover concentration during the Holocene in the Arctic

Ocean, the northern North Atlantic Ocean and its adjacent seas, Quaternary Sci. Rev., 79, 111-121, 2013.

Di Rita, F., and Magri, D.: The 4.2 ka BP event in the vegetation record of the central Mediterranean, Clim. Past, 15, 237-251, 2019.

Di Rita, F., Fletcher, W. J., Aranbarri, J., Margaritelli, G., Lirer, F., and Magri, D.: Holocene forest dynamics in central and western Mediterranean: periodicity, spatio-temporal patterns and climate influence, Sci. Rep.-UK, 8, 8929, https://doi.org/10.1038/s41598-018-27056-2, 2018.

Dixit, Y., Hodell, D. A., and Petrie, C. A.: Abrupt weakening of the summer monsoon in northwest India~ 4100 yr ago. Geology, 42, 339-342, 2014.

Donges, J. F., Donner, R., Marwan, N., Breitenbach, S. F., Rehfeld, K., and Kurths, J.: Non-linear regime shifts in Holocene Asian monsoon variability: potential impacts on cultural change and migratory patterns, Clim. Past, 11, 709-741, 2015.

Faegri, K. and Iversen, J.: Textbook of pollen analysis, 4th Ed., edited by: Faegri, K., Kaland, P. E., and Krzywinski, K., Wiley, Chichester, 1989.

Finné, M., Holmgren, K., Shen, C. C., Hu, H. M., Boyd, M., and Stocker, S.: Late Bronze Age climate change and the destruction of the Mycenaean Palace of Nestor at Pylos, PloS one, 12, e0189447. https://doi.org/10.1371/journal.pone.0189447, 2017.

Fisher, D., Osterberg, E., Dyke, A., Dahl-Jensen, D., Demuth, M., Zdanowicz, C., ... and Kreutz, K.: The Mt Logan Holocene—late Wisconsinan isotope record: tropical Pacific—Yukon connections, The Holocene, 18, 667-677, 2008.

Fohlmeister, J., Vollweiler, N., Spötl, C., and Mangini, A.: COMNISPA II: Update of a mid-European isotope climate record, 11 ka to present, The Holocene, 23, 749-754, 2013.

Häkkinen, S., Rhines, P. B., and Worthen, D. L.: Atmospheric blocking and Atlantic multidecadal ocean variability, Science, 334, 655-659, 2011.

Hátún, H., Sandø, A. B., Drange, H., Hansen, B., and Valdimarsson, H.: Influence of the Atlantic subpolar gyre on the thermohaline circulation, Science, 309, 1841-1844, 2005.

Ionita, M., Scholz, P., Lohmann, G., Dima, M., and Prange, M.: Linkages between atmospheric blocking, sea ice export through Fram Strait and the Atlantic Meridional Overturning Circulation, Nat. Sci. Rep., 6, 32881, 2016.

Jalali B, Sicre M.-A., Bassetti M.-A., and Kallel, N.: Holocene climate variability in the North-Western Mediterranean Sea (Gulf of Lions), Clim. Past 12, 91–101, 2016.

Jiang, H., Muscheler, R., Björck, S., Seidenkrantz, M. S., Olsen, J., Sha, L., ... & Knudsen, M. F.: Solar forcing of Holocene summer sea-surface temperatures in the northern North Atlantic, Geology, 43(3), 203-206, 2015.

Kissel, C., Van Toer, A., Laj, C., Cortijo, E., and Michel, E.: Variations in the strength of the North Atlantic bottom water during Holocene, Earth Planet. Sci. Lett., 369, 248-259, 2013.

Kobashi, T., Menviel, L., Jeltsch-Thömmes, A., Vinther, B. M., Box, J. E., Muscheler, R., ... and Wanner, H.: Volcanic influence on centennial to millennial Holocene Greenland temperature change, Nat. Sci. Rep., 1441, 2017.

Langehaug, H. R., Medhaug, I., Eldevik, T., and Otterå, O. H: Arctic/Atlantic exchanges via the subpolar gyre. J. Clim., 25, 2421-2439, 2012.

Liu, F., and Feng, Z.: A dramatic climatic transition at ~ 4000 cal. yr BP and its cultural responses in Chinese cultural domains, The Holocene, 22, 1181-1197, 2012.

Liu, Z., Yoshimura, K., Bowen, G. J., Buenning, N. H., Risi, C., Welker, J. M., and Yuan, F.: Paired oxygen isotope records reveal modern North American atmospheric dynamics during the Holocene, Nat. Commun., 5, 3701, doi: 10.1038/ncomms4701, 2014.

Locarnini, R. A., Mishonov, A. V., Antonov, J. I., Boyer, T. P., Garcia, H. E., Baranova, O. K., et al.: In S. Levitus (Ed.), technical ed A. Mishonov World Ocean Atlas 2013, Volume 1: Temperature

(Vol. 73, p. 40). MD: NOAA Atlas NESDIS. Retrieved from http://www.nodc.noaa.gov/OC5/indprod.html, 2013.

Luterbacher, J., Dietrich, D., Xoplaki, E., Grosjean, M., and Wanner, H.: European seasonal and annual temperature variability, trends, and extremes since 1500, Science, 30, 1499-1503, 2004.

Magny, M., Combourieu-Nebout, N., De Beaulieu, J. L., Bout-Roumazeilles, V., Colombaroli, D., Desprat, S., ... and Revel, M.: North-south palaeohydrological contrasts in the central Mediterranean during the Holocene: tentative synthesis and working hypotheses, Clim. Past, 9, 2043-2071, 2013.

Magri, D. and Sadori, L.: Late Pleistocene and Holocene pollen stratigraphy at Lago di Vico, central Italy, Veg. Hist. Archaeobot., 8, 247–260, 1999.

Magri, D.: Late Quaternary vegetation history at Lagaccione near Lago di Bolsena (central Italy), Rev. Palaeobot. Palyno., 106, 171–208, 1999.

Massé, G., Rowland, S., Sicre, M.-A., Jacob, J., Jansen, E. and Belt, S., Abrupt climate changes for Iceland during the last millennium: Evidence from high resolution sea ice reconstructions, Earth Planet. Sci. Lett. 269, 565-569, 2008.

Mayewski, P. A., Rohling, E. E., Stager, J. C., Karlén, W., Maasch, K. A., Meeker, L. D., ... and Lee-Thorp, J.: Holocene climate variability, Quaternary Res., 62, 243-255, 2004.

Mjell, T. L., Ninnemann, U. S., Eldevik, T., and Kleiven, H. K. F.: Holocene multidecadal-to millennial-scale variations in Iceland-Scotland overflow and their relationship to climate, Paleoceanography, 30, 558-569, 2015.

Moffa-Sánchez, P., Born, A., Hall, I. R., Thornalley, D. J., and Barker, S.: Solar forcing of North Atlantic surface temperature and salinity over the past millennium, Nature Geosci., 7, 275, 2014.

Moreno-Chamarro, E., Schmiedl, G., and Jungclaus, J. H.: Climate and ocean variability during the last millennium in paleo-observations and Earth system model simulations (Doctoral dissertation, Universität Hamburg, Hamburg), 2016.

Moreno-Chamarro, E., Zanchettin, D., Lohmann, K., Luterbacher, J., and Jungclaus, J. H.: Winter amplification of the European Little Ice Age cooling by the subpolar gyre, Scientific Reports, 7, 9981, 2017.

Nakamura, A., Yokoyama, Y., Maemoku, H., Yagi, H., Okamura, M., Matsuoka, H., ... and Ikehara, M.: Weak monsoon event at 4.2 ka recorded in sediment from Lake Rara, Himalayas, Quaternary Int., 397, 349-359, 2016.

Ning, L., Liu, J., Bradley, R. S., and Yan, M.: Comparing the spatial patterns of climate change in the 9th and 5th millennia B.P. from TRACE-21 model simulations, Clim. Past, 15, 41-52, 2019.

O'Brien, S. R., Mayewski, P. A., Meeker, L. D., Meese, D., Twickler, M. S., and Whitlow, S. I.: Complexity of Holocene climate as reconstructed from a Greenland ice core, Science, 270, 1962-1964, 1995.

Prahl, F.G., Muehlhausen, L.A., and Zahnle, D.L.: Further evaluation of longchain alkenones as indicators of paleoceanographic conditions, Geochim. Cosmochim. Acta 52, 2303–2310, 1988.

Quezel, P.: La région méditerranéenne française et ses essences forestières, signification écologique dans le contexte circumméditerranéen, Forêt Méd, 1, 7–18, 1979.

Ramsey, B.C.: Methods for Summarizing Radiocarbon Datasets, Radiocarbon, 59(2), 1809-1833, 2017.

Ran, L., Jiang, H., Knudsen, K. L., and Eiriksson, J.: A high-resolution Holocene diatom record on the North Icelandic shelf, Boreas, 37, 399-413, 2008.

Reille, M.: Pollen et Spores d’Europe et d’Afrique du Nord, Marseille: Laboratoire de Botanique historique et Palynologie, 520 pp., 1992.

Reimer, P. J., Bard, E., Bayliss, A., Beck, J. W., Blackwell, P. G., Ramsey, C. B., ... & Grootes, P. M.: IntCal13 and Marine13 radiocarbon age calibration curves 0–50,000 years cal BP, Radiocarbon, 55(4), 1869-1887, 2013.

Ruan, J., Kherbouche, F., Genty, D., Blamart, D., Cheng, H., Dewilde, F., ... and Michelot, J. L.: Evidence of a prolonged drought ca. 4200 yr BP correlated with prehistoric settlement abandonment from the Gueldaman GLD1 cave, Northern Algeria, Clim. Past, 12, 1-14, 2016.

Sha, L., Jiang, H., Seidenkrantz M.-S., Muscheler R., Zhang, X., Knudsen M.F., Olsen J., Knudsen, K.L., and Zhang W., Solar forcing as an important trigger for West Greenland sea-ice variability over the last mellennium, Quaternary Sci. Rev., 131, 148-156, 2016.

Sicre, M. A., Jalali, B., Martrat, B., Schmidt, S., Bassetti, M. A., and Kallel, N.: Sea surface temperature variability in the North Western Mediterranean Sea (Gulf of Lion) during the Common Era, Earth Planet. Sci. Lett., 456, 124-133, 2016.

Sicre, M-A., P. Yiou, J. Eiriksson, U. Ezat, E. Guimbaut, I. Dahhaoui, K.-L. Knudsen, E. Jansen, J.-L. Turon, A 4500-year reconstruction of sea surface temperature variability at decadal time scales off North Iceland, Quaternary Sci. Rev. 27, 2041-2047, 2008.

Solignac, S., de Vernal, A., and Hillaire-Marcel, C.: Holocene sea-surface conditions in the North Atlantic—contrasted trends and regimes in the western and eastern sectors (Labrador Sea vs. Iceland Basin), Quaternary Sci. Rev., 23, 319-334, 2004.

Solignac, S., Giraudeau, J., & de Vernal, A.: Holocene sea surface conditions in the western North Atlantic: spatial and temporal heterogeneities, Paleoceanography, 21(2), 2006.

Stanley J, Krom M, Cliff R et al.: Nile flow failure at the end of the Old Kingdom, Egypt: Strontium isotopic and petrologic evidence, Geoarchaeology 18, 395–402, 2003.

Ternois, Y, Sicre M.-A., Boireau A., Conte M.H. and Eglinton G.: Evaluation of long-chain alkenones as paleo-temperature indicators in the Mediterranean Sea, Deep Sea Research, 44, 271-286, 1997.

Thornalley, D. J., Elderfield, H., and McCave, I. N.: Holocene oscillations in temperature and salinity of the surface subpolar North Atlantic, Nature, 457, 711, 2009.

Walker, M.J., Berkelhammer, M., Björck, S., Cwynar, L.C., Fisher, D.A., Long, A.J., Lowe, J.J., Newnham, R.M., Rasmussen, S.O. and Weiss, H.: Formal subdivision of the Holocene Series/Epoch: a Discussion Paper by a Working Group of INTIMATE (Integration of ice-core, marine and terrestrial records) and the Subcommission on Quaternary Stratigraphy (International Commission on Stratigraphy), J. Quaternary Sci., 27, 649-659, 2012.

Wanner, H., Mercolli, L., Grosjean, M., and Ritz, S. P.: Holocene climate variability and change; a data-based review. J. of the Geol. Soc, 172, 254-263, 2014.

Wanner, H., Solomina, O., Grosjean, M., Ritz, S. P., and Jetel, M.: Structure and origin of Holocene cold events, Quaternary Sci. Rev., 30, 3109-3123, 2011.

Weiss, H., and Bradley, R. S.: What drives societal collapse?, Science, 29, 609-610, 2001.

Weiss, H.: Global megadrought, societal collapse and resilience at 4.2-3.9 ka BP across the Mediterranean and west Asia, PAGES Magazine, 24, 62-63, 2016.

Weiss, H.: Megadrought, collapse, and resilience in late 3rd millennium BC Mesopotamia. In book: Meller, H., Arz, H. W., Jung, R., and Risch, R., eds, 2200 BC – A climatic breakdown as a cause for collapse of the Wold World? Halle: Landesmuseum fur Vorgeschichte, 35-52, 2015.

Yan, M. and Liu J.: Physical processes of cooling and mega-drought during the 4.2 ka BP event: results from TraCE-21ka simulations, Clim. Past, 15, 265–277, 2019.

Zanchetta, G., Regattieri, E., Isola, I., Drysdale, R. N., Bini, M., Baneschi, I., and Hellstrom, J. C.: The so-called "4.2 event" in the central Mediterranean and its climatic teleconnections, Alp Mediterr. Quaternary, 29, 5-17, 2016.

Table S1: Age models of the MD95-2015 and KSGC-31 sediment cores. Radiocarbon ages have been calibrated using the Bayesian approach of OxCal4.3 software (Ramsey, 2017), the MARINE13 calibration data set (Reimer et al., 2013) and a ΔR = 73±69 for MD95-2015 and 23±71 for KSGC31 obtained from the Global Marine Reservoir Database using the eight nearest reservoir ages (http://calib.org/marine/).

Core	Depth (cm)	Lab. No.	Material	^{14}C Ages (BP) ± 1 Sigma	Modelled Age (Cal BP) ± 1 Sigma
MD95-2015	0.5		Core Top		680 ± 194
MD95-2015	10	LMC14-96590	*Globigerina bulloides*	1350 ± 60	813 ± 92
MD95-2015	30	LMC14-99350	*Globigerina bulloides*	1790 ± 60	1231 ± 94
MD95-2015	60	LMC14-96591	*Globigerina bulloides*	2220 ± 60	1704 ± 110
MD95-2015	90	LMC14-99351	*Globigerina bulloides*	2960 ± 60	2605 ± 118
MD95-2015	110	LMC14-96592	*Globigerina bulloides*	3390 ± 60	3103 ± 124
MD95-2015	150	LMC14-99352	*Globigerina bulloides*	4060 ± 60	3941 ± 128
MD95-2015	200	LMC14-96593	*Globigerina bulloides*	4660 ± 70	4762 ± 131
MD95-2015	240	LMC14-96598	*Globigerina bulloides*	5310 ± 80	5579 ± 119
MD95-2015	260	LMC14-99353	*Globigerina bulloides*	5980 ± 70	6283 ± 107
MD95-2015	290	LMC14-99354	*Globigerina bulloides*	6570 ± 70	6955 ± 122
MD95-2015	310	LMC14-99355	*Globigerina bulloides*	6850 ± 80	7244 ± 108
MD95-2015	390	LMC14-96599	*Globigerina bulloides*	7540 ± 90	7927 ± 116
MD95-2015	390	LMC14-99357	*Globigerina bulloides*	7950 ± 90	8292 ± 116
MD95-2015	420	LMC14-99358	*Globigerina bulloides*	8370 ± 100	8768 ± 134
MD95-2015	440	LMC14-96600	*Globigerina bulloides*	8560 ± 80	8989 ± 134
MD95-2015	480	LMC14-99359	*Globigerina bulloides*	8660 ± 90	9236 ± 117
MD95-2015	500	LMC14-96601	*Globigerina bulloides*	8840 ± 90	9385 ± 112
MD95-2015	600	LMC14-96602	*Globigerina bulloides*	9540 ± 90	10252 ± 130
MD95-2015	700	LMC14-96603	*Globigerina bulloides*	9940 ± 90	10891 ± 144
MD95-2015	749	LMC14-96604	*Globigerina bulloides*	11590 ± 90	12932 ± 127
MD95-2015	790	LMC14-96605	*Globigerina bulloides*	12270 ± 100	13622 ± 137
KSGC-31	0.5		Core Top		-21

KSGC-31	25.5	LMC14	*Venus* sp.	640 ± 30	224 ± 90
KSGC-31	41	LMC14	*Pecten* sp.	700 ± 30	325 ± 80
KSGC-31	52	LMC14	Indet. bivalve	960 ± 30	523 ± 58
KSGC-31	71	LMC14	*Arca tetragona*	1340 ± 30	807 ± 78
KSGC-31	110.5	LMC14	*Venus* sp.	1465 ± 30	995 ± 86
KSGC-31	186.5	LMC14	*Nucula* sp	2235 ± 40	1797 ± 97
KSGC-31	251	LMC14	Juvenile bivalve shells (ind.)	2940 ± 30	2670 ± 92
KSGC-31	330.5	LMC14	*Venus casina*	3870 ± 30	3775 ± 103
KSGC-31	370.5	LMC14	*Nuculana* sp.	4170 ± 30	4210 ± 112
KSGC-31	390.5	LMC14	*Turritella* sp.	4500 ± 30	4629 ± 111
KSGC-31	460	LMC14	*Venus* sp.	5530 ± 45	5876 ± 98
KSGC-31	481	LMC14	*Ostrea* sp	5955 ± 35	6328 ± 79
KSGC-31	501.5	LMC14	*Turritella* sp.	6380 ± 50	6790 ± 103
KSGC-31	552	LMC14	Shells (mixed)	7215 ± 30	7641 ± 73
KSGC-31	583	LMC14	*Turritella* sp.	7860 ± 60	8239 ± 99
KSGC-31	652	LMC14	*Turritella* sp.	8310 ± 35	8852 ± 117
KSGC-31	701	LMC14	*Turritella* sp.	9190 ± 50	9867 ± 148

Figure captions

Figure 1: Map of the annual mean SSTs (1955–2012) from World Ocean Atlas database (https://data.nodc.noaa.gov/las/getUI.do; Locarnini et al., 2013) showing the location of the investigated cores and sites used for comparison. (1) marine core MD95-2015 (this study); (2) marine core MD99-2275 (this study); (3) marine core GS06-144 08GC (Mjell et al., 2015); (4) marine core RAPiD-12-1K (Thornalley et al., 2009); (5) marine core P-013 (Solignac et al., 2004); (6) marine core JM96 1207 (Solignac et al., 2006); (7) ice core GISP2 (O'Brien et al., 1995); (8) marine core Fox05R/04G (Andresen et al., 2012); (9) marine core MD95-2011 (Berner et al., 2011); (10) marine core KSGC-31 (Jalali et al., 2016); (11) Core PB06 from the Palavasian Lagoon (Azuara et al., 2015); (12) Speleothem from Renella Cave (Zanchetta et al., 2016); (13) Speleothem from Gueldaman Cave (Ruan et al., 2016). Subpolar and subtropical gyres as well as main surface currents in the North Atlantic are also shown. IC: Irminger Current; NIIC: North Icelandic Irminger Current; EIC: East Icelandic Current; EGC: East Greenland Current.

Figure 2: Alkenone-derived Sea surface temperatures (SSTs) in the North Atlantic cores between 5500 and 2500 Cal yr BP. (a) at the MD95-2015 core (site 1 in Fig. 1) and (b) at the MD99-2275 core (site 2 in Fig. 1). (c) C_{37} alkenone concentrations (in ng/g dry sediment) at the MD95-2015 core (d) and MD99-2275 core. 50 years binning is applied to reduce the effect of proxy reconstruction error (thick lines). The grey vertical band represents the 4.2 ka BP event time-interval (4400-3800 Cal. yr BP).

Figure 3: Paleoclimatic and paleoceanographic data from the North Atlantic during the 4.2 ka BP event. (a) Alkenone-derived SSTs at the MD95-2015 core. (b) Alkenone-derived SSTs at the MD99-2275 core. (c) Density difference between surface and subsurface waters obtained from paired Mg/Ca and $\delta^{18}O$ in *Globigerina bulloides* and *Globorotalia inflata* in core RAPiD-12-1K (site 4 in Fig. 1) (Thornalley et al., 2009). (d) Mean sortable silt (SS, 10-63µm) in core GS06-144 08GC in the Iceland Basin (site 3, Fig. 1) (Mjell et al., 2015). (e) Sea-salt Na flux from GISP2 ice core (site 7, Fig. 1) (O'Brien et al., 1995). (f) Sea ice concentration from the East Greenland shelf based on dinoflagellate cyst assemblages in core JM96 1207 (site 6, Fig. 1) (Solignac et al., 2006). (g) Dinoflagellate cyst assemblages inferred sea surface salinity from the Labrador Sea core P-013 (site 5, Fig. 1) (Solignac et al., 2004). (h) Summer SSTs derived from diatom based weighted averaging partial least squares transfer function from core MD95-2011 (site 9, Fig.1) (Berner et al., 2011). For (a), (b) and (d) 50 years

binning is applied to reduce the effect of proxy reconstruction error (thick lines). This binning has not been applied on the low temporal resolution records. The grey vertical band represents the 4.2 ka BP event time-interval (4400-3800 yr BP). The dashed line highlights the 4100 yr BP where extrema are seen in most records.

Figure 4: Expression of the 4.2 ka BP event in the W Mediterranean region as recorded by marine and continental archives. (a) Alkenone SSTs at the KSGC-31 core in the Gulf of Lion (site 10, Fig. 1, Jalali et al., 2016). (b) Log *Fagus*/ deciduous *Quercus* in the KSGC-31 core (this study). (c) Log *Fagus*/ deciduous *Quercus* in core PB06 from the Palavasian Lagoon (site 11, Fig. 1, Azuara et al., 2015). (d) Alkenone SSTs at the MD99-2275 core (site 2, Fig. 1) (North Iceland; this study). (e) $\delta^{18}O$ record obtained from Renella Cave stalagmite (site 12, Fig. 1) (North Italy; Zanchetta et al., 2016). (f) $\delta^{18}O$ record obtained from Gueldaman Cave stalagmite (site 13, Fig. 1) (Algeria; Ruan et al., 2016). A 50 years binning is applied to reduce the effect of proxy reconstruction error (thick lines). The grey vertical band represents the 4.2 ka BP event time-interval (4400-3800 yr BP).

Figure S1: Age model of the core MD95-2015 calculated using the Bayesian Oxcal4.3 software (Ramsey, 2017), the MARINE13 calibration data set (Reimer et al., 2013) and a $\Delta R = 73\pm69$ calculated as the mean value of the eight nearest site reservoir ages obtained from the Global Marine Reservoir Database (http://calib.org/marine/). The green lines represent 1σ age uncertainty.

Figure S2: Age model of the core KSGC-31 calculated using the Bayesian Oxcal4.3 software (Ramsey, 2017), the MARINE13 calibration data set (Reimer et al., 2013) and a $\Delta R = 23\pm71$ calculated as the mean value of the eight nearest reservoir ages obtained from the Global Marine Reservoir Database (http://calib.org/marine/). The blue lines represent 1σ age uncertainty.

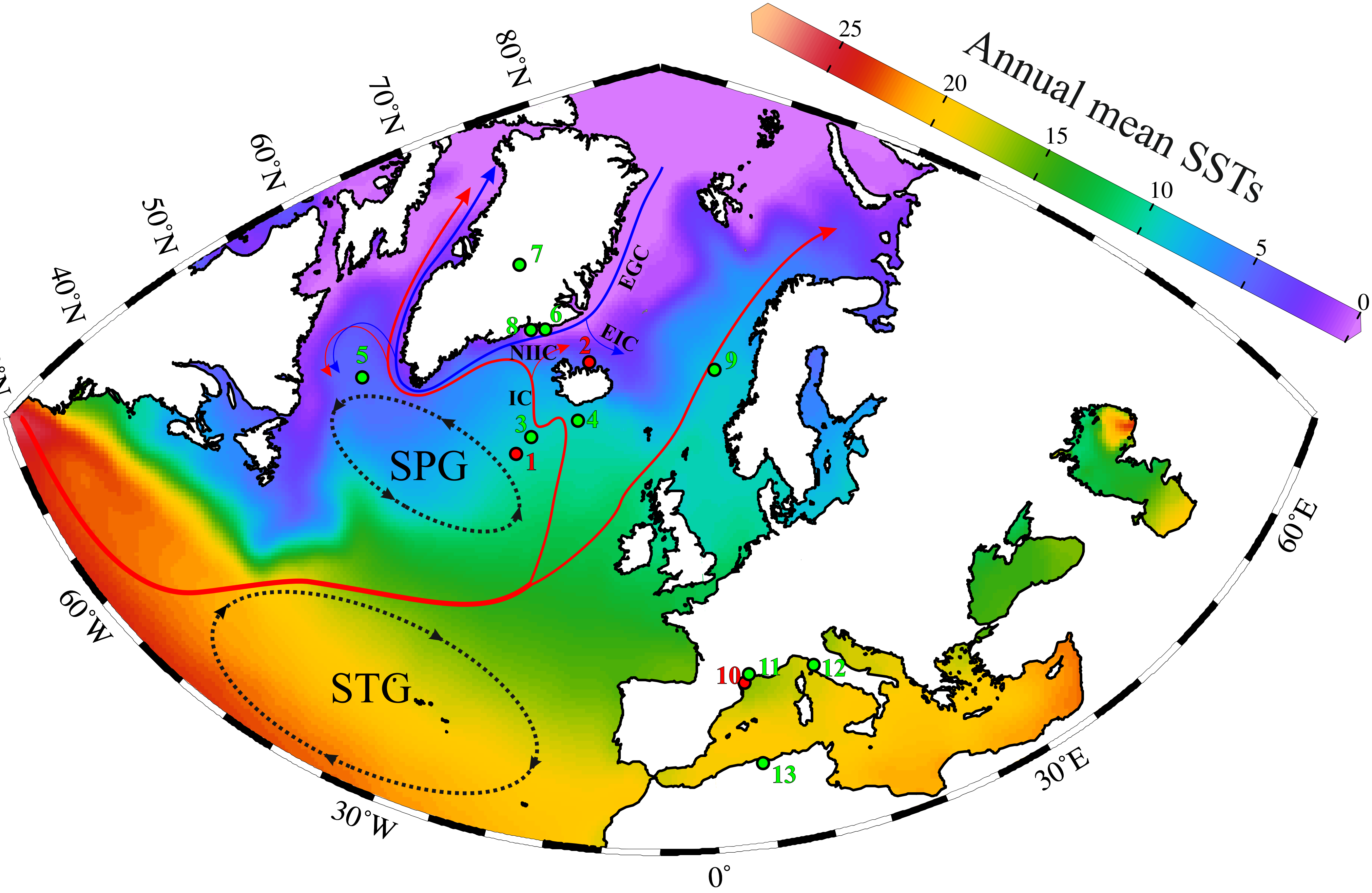
Annual mean SSTs
25
20
15
10
5
0
30°N
40°N
50°N
60°N
70°N
80°N
60°W
30°W
0°
30°E
60°E
SPG
STG
EGC
EIC
NIIC
IC
1
2
3
4
5
6
7
8
9
10
11
12
13

Figure 1

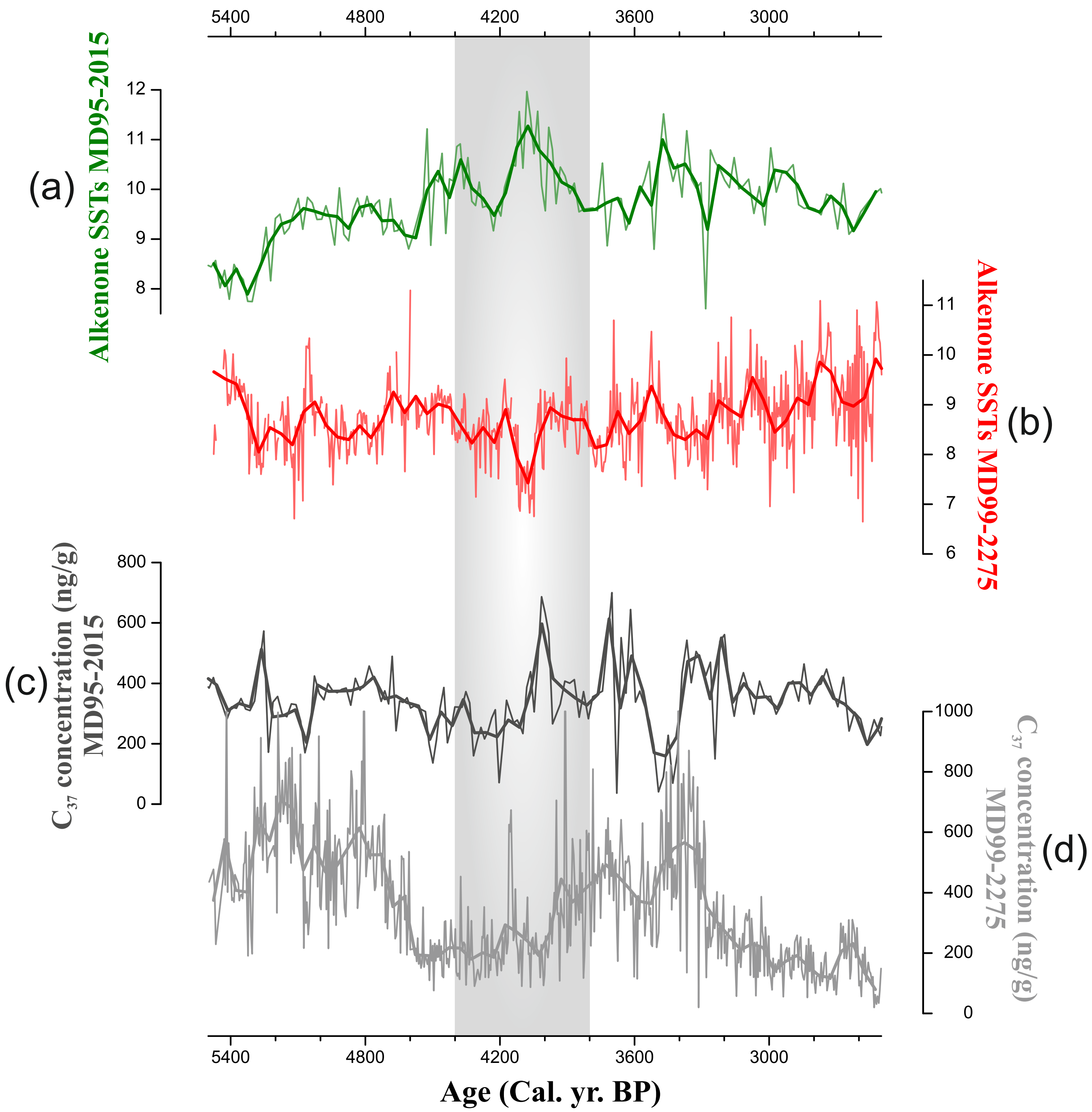

5400
4800
4200
3600
3000
(a)
Alkenone SSTs MD95-2015
12
11
10
9
8
Alkenone SSTs MD99-2275
11
10
9
8
7
6
(b)
(c)
C_{37} concentration (ng/g) MD95-2015
800
600
400
200
0
1000
800
600
400
200
0
C_{37} concentration (ng/g) MD99-2275
(d)
Age (Cal. yr. BP)

Figure 2

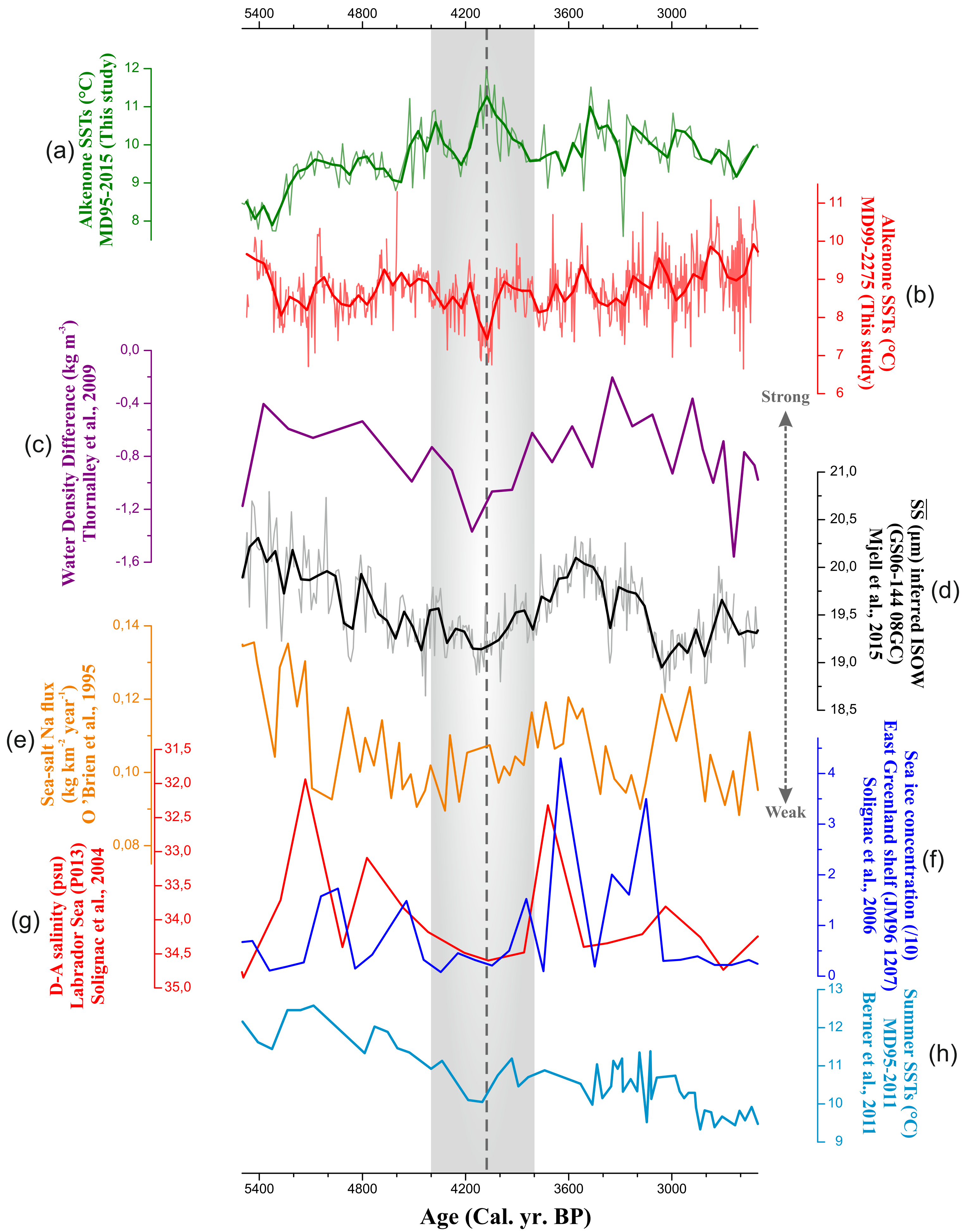

Age (Cal. yr. BP)
(a)
Alkenone SSTs (°C)
MD95-2015 (This study)
(b)
Alkenone SSTs (°C)
MD99-2275 (This study)
(c)
Water Density Difference (kg m-3)
Thornalley et al., 2009
(d)
SS (µm) inferred ISOW
(GS06-144 08GC)
Mjell et al., 2015
Strong
Weak
(e)
Sea-salt Na flux
(kg km-2 year-1)
O 'Brien et al., 1995
(f)
Sea ice concentration (/10)
East Greenland shelf (JM96 1207)
Solignac et al., 2006
(g)
D-A salinity (psu)
Labrador Sea (P013)
Solignac et al., 2004
(h)
Summer SSTs (°C)
MD95-2011
Berner et al., 2011

Figure 3

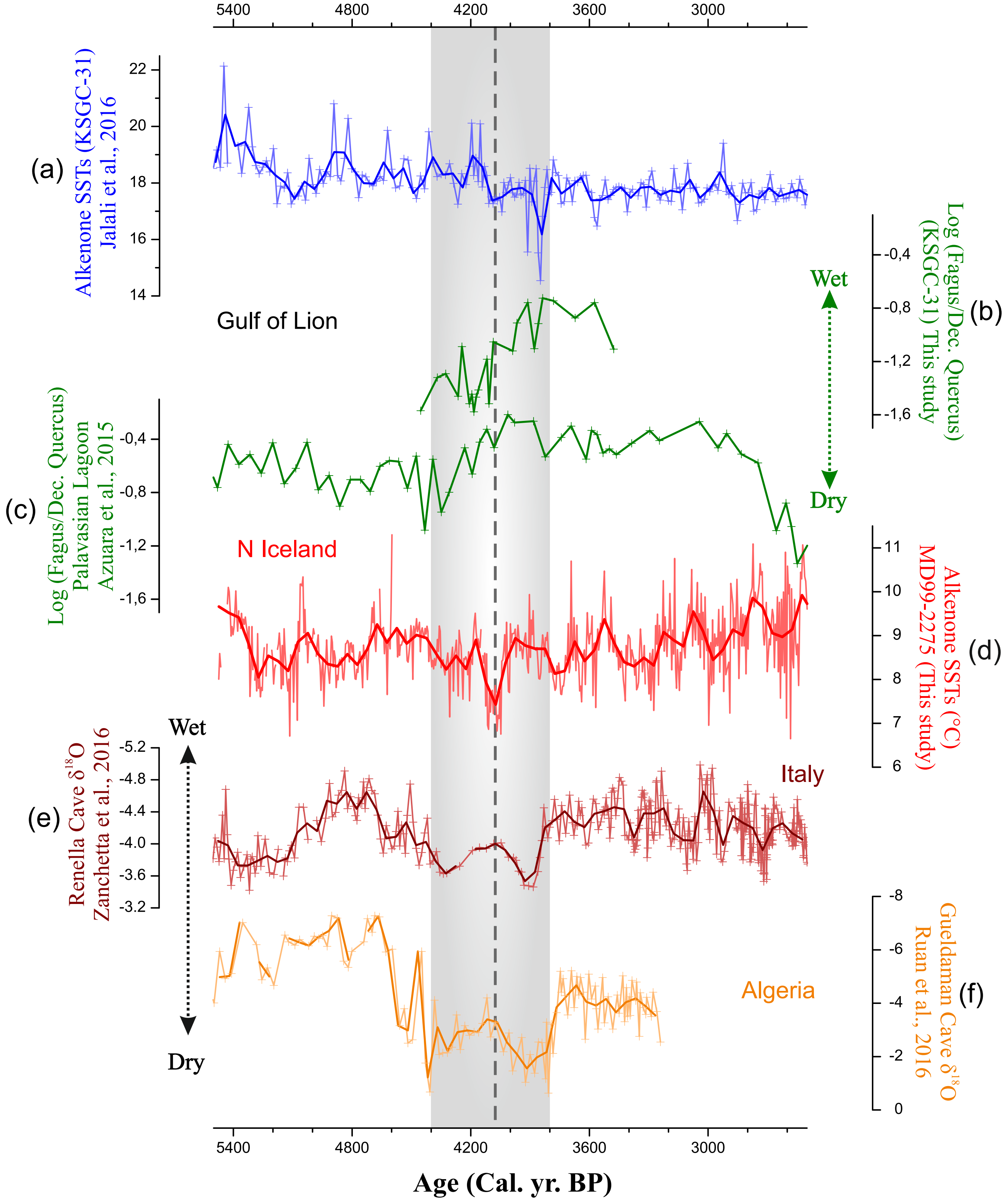

5400
4800
4200
3600
3000
(a)
Alkenone SSTs (KSGC-31)
Jalali et al., 2016
22
20
18
16
14
Gulf of Lion
Log (Fagus/Dec. Quercus)
(KSGC-31) This study
(b)
-0,4
-0,8
-1,2
-1,6
Wet
Dry
(c)
Log (Fagus/Dec. Quercus)
Palavasian Lagoon
Azuara et al., 2015
-0,4
-0,8
-1,2
-1,6
N Iceland
Alkenone SSTs (°C)
MD99-2275 (This study)
(d)
11
10
9
8
7
6
(e)
Renella Cave δ18O
Zanchetta et al., 2016
-5.2
-4.8
-4.4
-4.0
-3.6
-3.2
Wet
Dry
Italy
Algeria
Gueldaman Cave δ18O
Ruan et al., 2016
(f)
-8
-6
-4
-2
0
Age (Cal. yr. BP)

Figure 4

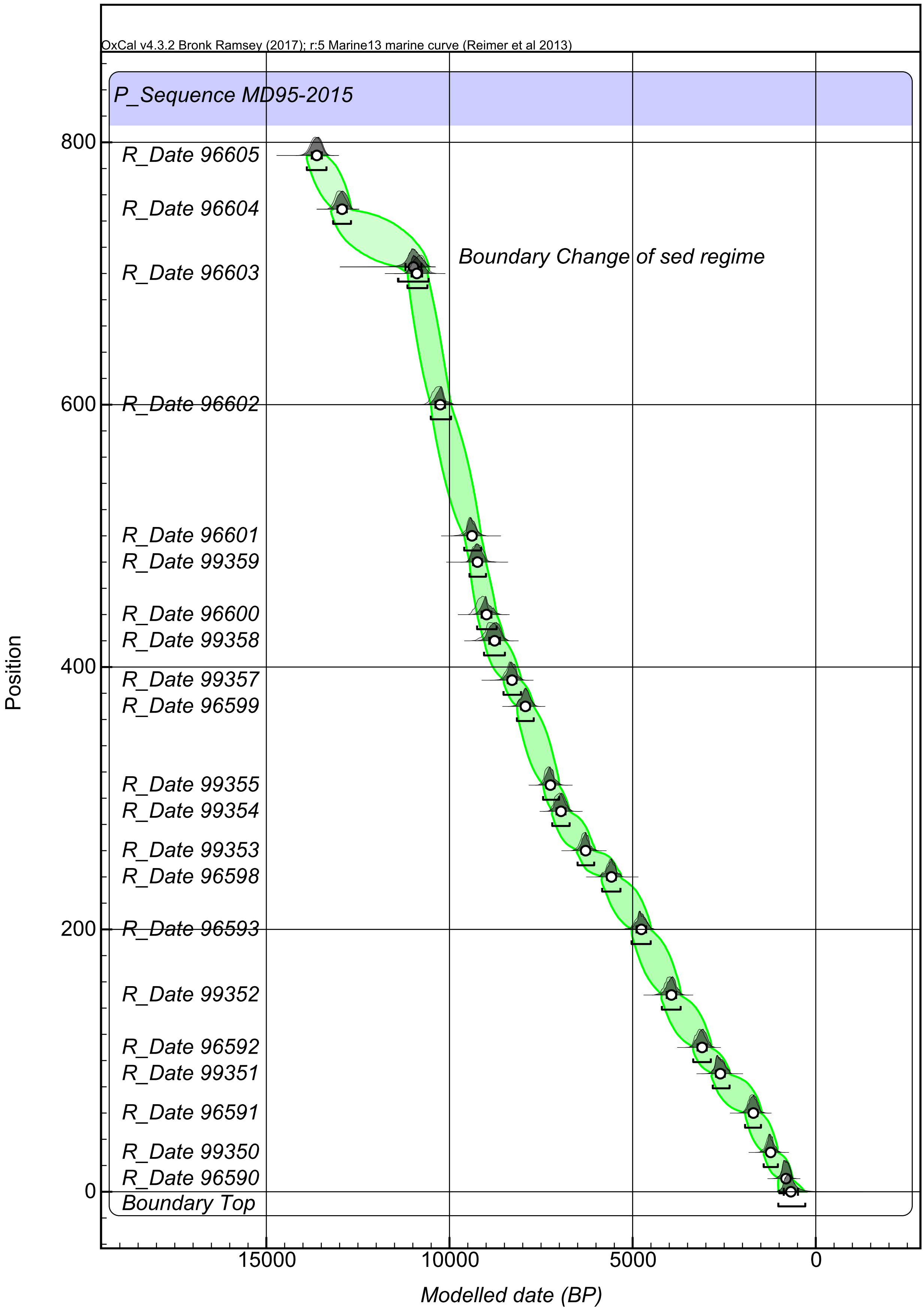
OxCal v4.3.2 Bronk Ramsey (2017); r:5 Marine13 marine curve (Reimer et al 2013)
P_Sequence MD95-2015
R_Date 96605
R_Date 96604
Boundary Change of sed regime
R_Date 96603
R_Date 96602
R_Date 96601
R_Date 99359
R_Date 96600
R_Date 99358
R_Date 99357
R_Date 96599
R_Date 99355
R_Date 99354
R_Date 99353
R_Date 96598
R_Date 96593
R_Date 99352
R_Date 96592
R_Date 99351
R_Date 96591
R_Date 99350
R_Date 96590
Boundary Top
800
600
400
200
0
Position
15000
10000
5000
0
Modelled date (BP)

Figure S1

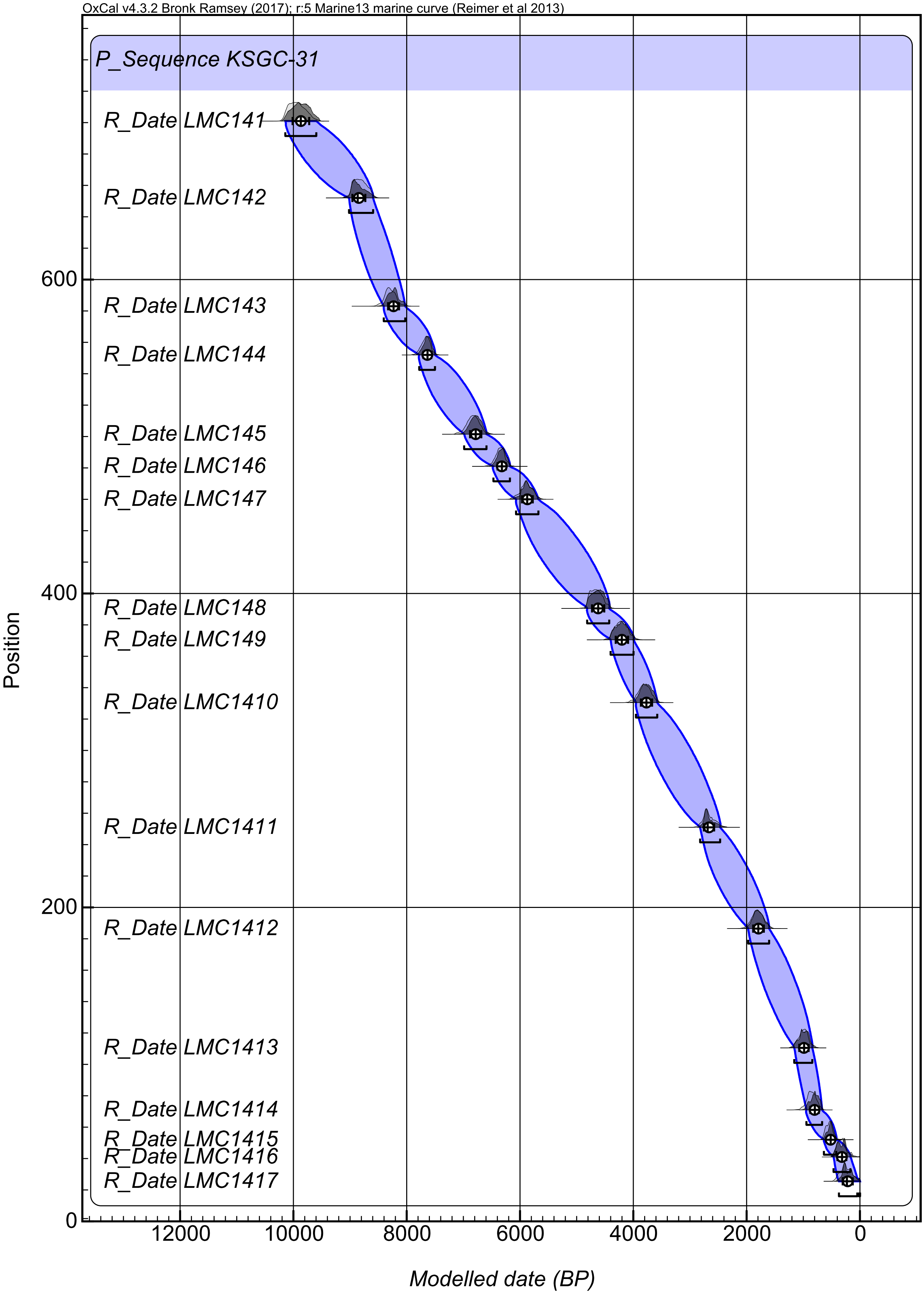

OxCal v4.3.2 Bronk Ramsey (2017); r:5 Marine13 marine curve (Reimer et al 2013)
P_Sequence KSGC-31
R_Date LMC141
R_Date LMC142
R_Date LMC143
R_Date LMC144
R_Date LMC145
R_Date LMC146
R_Date LMC147
R_Date LMC148
R_Date LMC149
R_Date LMC1410
R_Date LMC1411
R_Date LMC1412
R_Date LMC1413
R_Date LMC1414
R_Date LMC1415
R_Date LMC1416
R_Date LMC1417
600
400
200
0
Position
12000
10000
8000
6000
4000
2000
0
Modelled date (BP)

Figure S2